Laser Holographic Interferometry for an Unsteady Airfoil Undergoing Dynamic Stall

George Lee,* Donald A. Buell,† and Joseph P. Licursi‡
NASA Ames Research Center, Moffett Field, California
and
James E. Craig†
Spectron Development Laboratory, Costa Mesa, Calif.

Laser holographic interferometry was used to study a two-dimensional NACA 0012 airfoil undergoing dynamic stall. The airfoil, fabricated from graphite fiber and epoxy, was tested at Mach numbers of 0.3-0.6, Reynolds numbers of 0.5×10^6 to 2.0×10^6, reduced frequencies of 0.015-0.15, and mean angles of attack of 0-10 deg with amplitudes of 10 deg. Density and pressure fields were obtained from dual-plate interferograms. Double-pulse interferograms, which seemed to show the wake boundaries better, were also taken. Comparisons of pressures with orifice pressures were good for the attached flow cases. For the separated flow cases, which had a vortex embedded in the flow, the comparisons were poor. Vortices, wake structures, and the dynamic stall process can be seen by holographic interferometry.

Nomenclature

c = chord of airfoil
C_p = pressure coefficient
k = reduced frequency
L = width of test section
M = Mach number
n = refractive index of air
N = fringe number
r = recovery factor, 0.88
T = temperature
u = velocity
x,y,z = Cartesian coordinates
α = angle of attack
γ = specific heat ratio
$\Delta\Phi$ = fringe shift
κ = Gladstone-Dale constant
δ = thickness of boundary layer or separated region
λ = wavelength of laser light
ρ = density

Subscripts

ad = adiabatic wall condition
e = boundary-layer edge conditions
0 = reference condition
w = wall condition

Introduction

In the past few years, laser holographic interferometry has been shown to be a valuable diagnostic tool for wind tunnel studies of steady two-dimensional flows. The entire density fields can be visualized easily and mapped quantitatively without disturbance, since only light is used to probe the flow. For the special case of infinite fringe interferograms of two-dimensional flows, the fringe lines become lines of constant density. Thus, density contours are obtained directly. With the assumption of isentropic flow, Mach number and velocity contours, which are commonly used to verify aerodynamic codes, as well as surface pressures, can be deduced from the density data. Other aerodynamic parameters of interest, such as shock waves, boundary layers, wakes, regions of separated flow, and the shedding of large scale vortices, can also be visualized using this technique.

Because of the success of laser holographic interferometry for steady two-dimensional flows, an experiment was designed to determine the feasibility of the technique for application to unsteady two-dimensional flows. For this experiment, the unsteady flow over an airfoil undergoing dynamic stall was considered since the unsteady flow effects are large. Many different types of flows occur as the airfoil goes through an oscillation. At low angles of attack, the flow is attached on the upper suface; but as the angle of attack is increased, the flow begins to separate. Small vortices appear near the onset of stall and a large dynamic stall vortex sheds across the airfoil during deep stall. Then, as the airfoil goes through decreasing angles of attack, there is a complex reattachment process.

Previous flow visualization studies of airfoils undergoing dynamic stall have been made in both air and water. The smoke technique[1] has been used in air to visualize the streamlines, the vortices, and the flow processes occurring around an airfoil as it goes through dynamic stall. Tufts, attached to the airfoil, have also been used to observe the flow reversal process on airfoils. Similarly, dyes and polystyrene beads,[2] air bubbles,[3] and hydrogen bubbles[4] have been used in water tunnels to make the flow visible. The bubbles, bead, and hydrogen methods show the smaller vortices quite well, and the smoke and dye methods show the larger-scale flow structures, such as the dynamic stall vortex. The main drawback of all these methods is that they are qualitative in nature. One of the many advantages of laser holographic interferometry for studying dynamic stall and other unsteady flows in that it is a quantitative measurement technique. Short laser pulses (of the order of nanoseconds) can freeze unsteady flow patterns for subsequent quantitative analysis. Moreover, the technique is very sensitive and small density variations can be measured. In the present experiment, an existing laser holographic interferometer was synchronized to an oscillating airfoil to demonstrate laser holographic interferometry as both a quantitative and qualitative visualization technique for unsteady two-dimensional flows.

Submitted Feb. 4, 1983; revision submitted June 6, 1983. This paper is declared a work of the U.S. Government and therefore is in the public domain.

*Assistant Chief, Aerodynamics Research Branch. Member AIAA.
†Research Scientist.
‡Technician.

Table 1 Theoretical and measured airfoil coordinates

Chord station, %	Specified thickness, % of chord	Measured thickness, %of chord	
		Upper	Lower
0.78	1.52	1.44	1.82
1.77	2.23	2.15	2.53
3.97	3.27	3.14	3.52
8.22	4.35	4.31	4.65
17.30	5.55	5.58	5.84
29.28	6.00	6.07	6.24
46.42	5.50	5.64	5.68
63.18	4.29	4.42	4.38
75.13	3.15	3.27	3.15
87.47	1.76	1.92	1.72

Experiments

Model

The two-dimensional airfoil model tested was a nominal NACA 0012 section with a 15.24 cm (6.00 in.) chord. In order to have a light, strong structure suitable for efficient oscillatory motion, the airfoil was fabricated from 20 plies of graphite tape impregnated with epoxy resin over a balsa wood core. The resulting surface had the smoothness of a polished metal surface; it was, however, somewhat thicker than planned, corresponding more nearly to a 12.5% section instead of the nominal 12%. See Table 1 for the actual airfoil coordinates.

The airfoil span was 61.0 cm (24.0 in.); it was mounted between the glass windows of the test section with a gap at each end of 1 mm (0.04 in.) or less. The wing was mounted in the windows by steel stubs that rode in needle bearings. All metal parts were kept as small as possible to reduce the inertial loads. The wing was pitched about the quarter-chord axis by oscillating the driving arm, through an eccentric arm, with a 110 hp, variable-frequency electric motor, as shown in Fig. 1. With this linkage, it was relatively easy to adjust the mean angle of attack, but a lengthy eccentric replacement was required to change amplitude. The motor was selected because of its large inertia, which minimized the effect of aerodynamic forces on the airfoil motion, and not because of its power rating, which greatly exceeded that required.

Spherical wing-window bearings were used to keep wing bending from imposing moments on the glass, and the driving arm was attached through a universal-type joint. It was, therefore, necessary to restrain the end of the driving arm in a phenolic laminate guide. Although there were some maintenance difficulties with the bearings and guide, the primary weakness in the model was subsequently found to be the joint between the steel stub and the carbon epoxy composite. A sketch of the wing is shown in Fig. 1b. The bonding at the joint on the nondriven end of the airfoil separated from the stainless steel stub (despite etching) after approximately 5×10^6 cycles, 3×10^6 of which occurred under significant aerodynamic loading.

Airfoil, Phase, and Position

A mechanical indication of phase was obtained from a segmented disk bolted onto the motor shaft. The disk pattern, consisting of one white segment in the inner track and 100 segments in the outer track, can be seen in Fig. 1. The intention was to have a positive indication of airfoil position vs time, whether or not the motor maintained a steady rotation. The segments on each track were transformed into electrical pulses by focusing the light from light-emitting diodes onto the disk and back onto photodetectors. After shaping, the pulses were then used to trigger data sampling. The primary problem with the system was an occasional loss of signal caused by losing the focus of the light-emitting diodes when the disk vibrated at some of the higher rotational speeds.

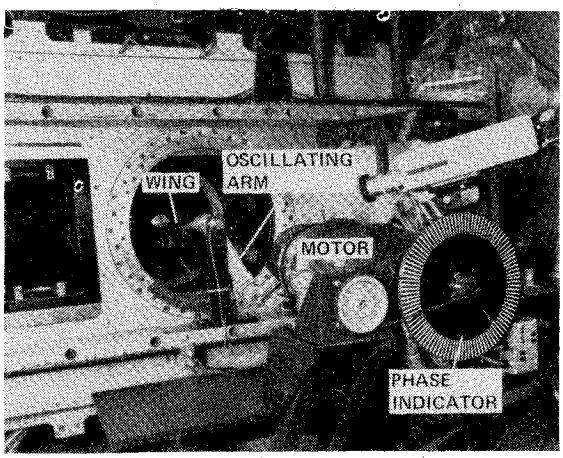

Fig. 1a Wind tunnel, wing, and oscillating mechanism.

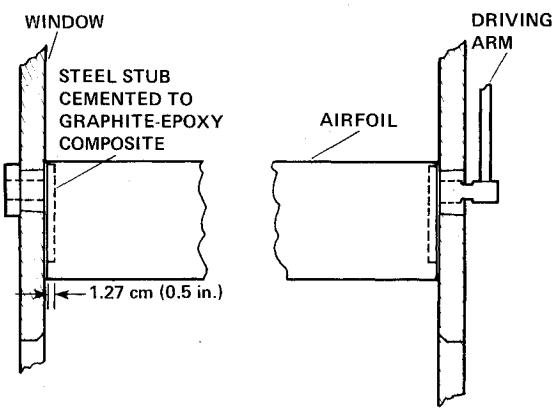

Fig. 1b Airfoil mounting.

The airfoil position was also determined from a rotary transformer that was mechanically coupled to the airfoil just outside the test section window. The unit can be seen in Fig. 1, with its mounting bracket partially obscuring the driving arm. The position signal was amplified and recorded on the same devices as the pressure transducers described below.

Pressures

Instantaneous pressures on the wing were measured with absolute-pressure, high-response transducers. The transducers, 1.3 mm (0.052 in.) in diameter, were mounted in plastic tubes under the composite skin and connected to the surface through 0.76 mm (0.030 in.) orifices. Nine transducers were installed in each surface.

The transducer signals were processed by a balancing circuit and a dc amplifier; they were then routed to monitoring circuits, a minicomputer, an analog FM tape recorder, and an oscillograph. The wing pressure signals were also passed to summing amplifiers for an on-line indication of lift and pitching moment.

Tests

The model was tested at Mach numbers of 0.3, 0.4, 0.5, and 0.6 at chord Reynolds numbers of 2×10^6. Reynolds numbers down to 0.5×10^6 were also tested. Tests with the airfoil stationary were conducted at angles of attack from -25 to $+20$ deg at 2.5 deg intervals, except at the stall angle where the wing (restrained at one end only) fluttered. Oscillatory tests were conducted with mean angles of attack of 5 and 10 deg at an amplitude of 10 deg at frequencies up to 36 Hz.

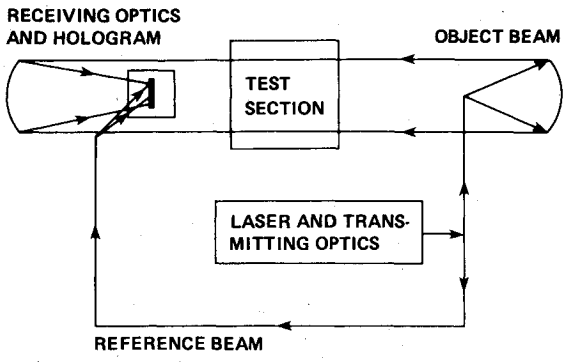

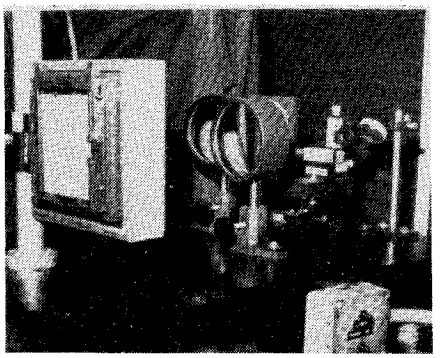

RECEIVING OPTICS AND HOLOGRAM

LASER AND TRANSMITTING OPTICS

Fig. 2 Interferometer (2×2 ft).

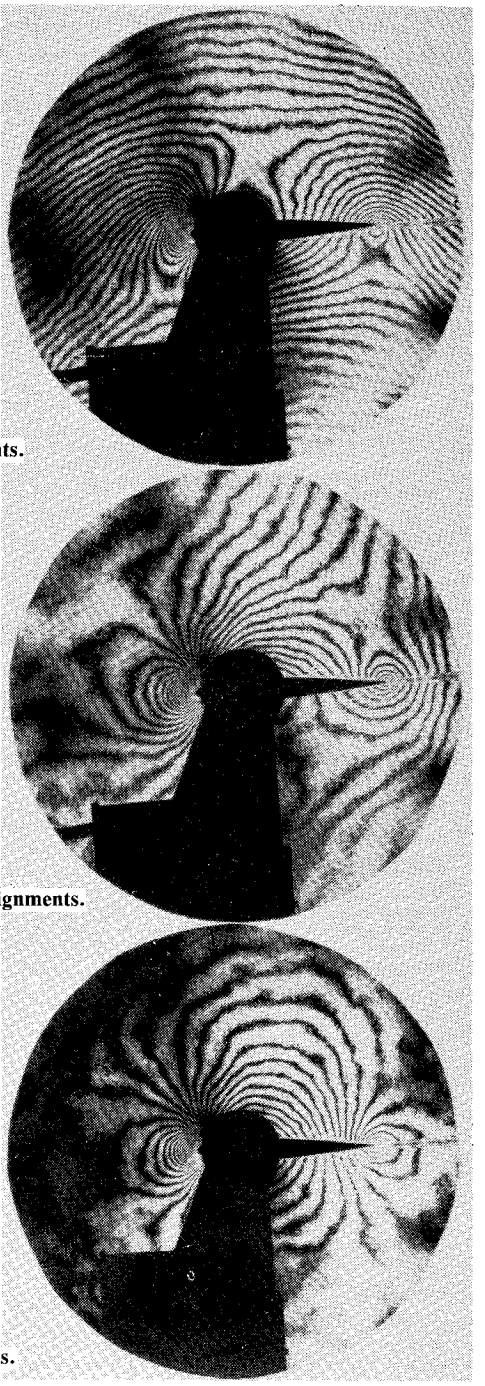

a) Initial alignments.

b) Intermediate alignments.

c) Final alignments.

Fig. 3 Reconstruction process of infinite fringe interferograms.

Holographic Interferometry

A basic description of holographic interferometry is given in many textbooks, for example, Ref. 5. In interferometry, two or more waves are superimposed; the resulting constructive and destructive interference causes bright and dark fringes, respectively. Holographic interferometry allows the storage of two waves separated in time to be superimposed in reconstruction. The two waves can be stored on a single hologram (double-pulse holographic interferometry) or on two separate plates (dual-plate holographic interferometry). The double-pulse technique is easily accomplished, but it is less flexible because the fringe spacing is fixed. The superimposed reconstruction waves are viewed directly and then photographed.

The double-pulse technique was used to study unsteady motions, and the information recorded is the change in densities that occurs during the time between the laser pulses. The data are qualitative in this case, because no reference density condition was available. The dual-plate technique is more difficult, but it is much more flexible than the double-pulse one. It is necessary to use this method when quantitative flowfield data are required. In using dual-plate holography, a reference exposure is recorded with no flow in the test field on the first film plate. Another exposure is recorded at test conditions on the second film plate. A special two-plate carrier used in the reconstruction system allows adjustment of the first film plate positon with respect to the second film plate. When the plates are repositioned correctly, the reconstructed wave fronts interfere to form a fringe pattern. If both holograms were recorded in the absence of aerodynamic flow, the reconstructed interferogram should exhibit broad fringe spacings, with only a few fringes in the field owing to slight misalignment and optical imperfections. When one of the holograms is recorded in the presence of aerodynamic flow, the fringes (being contours of constant-phase shift) represent constant-density contours in the special case of two-dimensional flows.

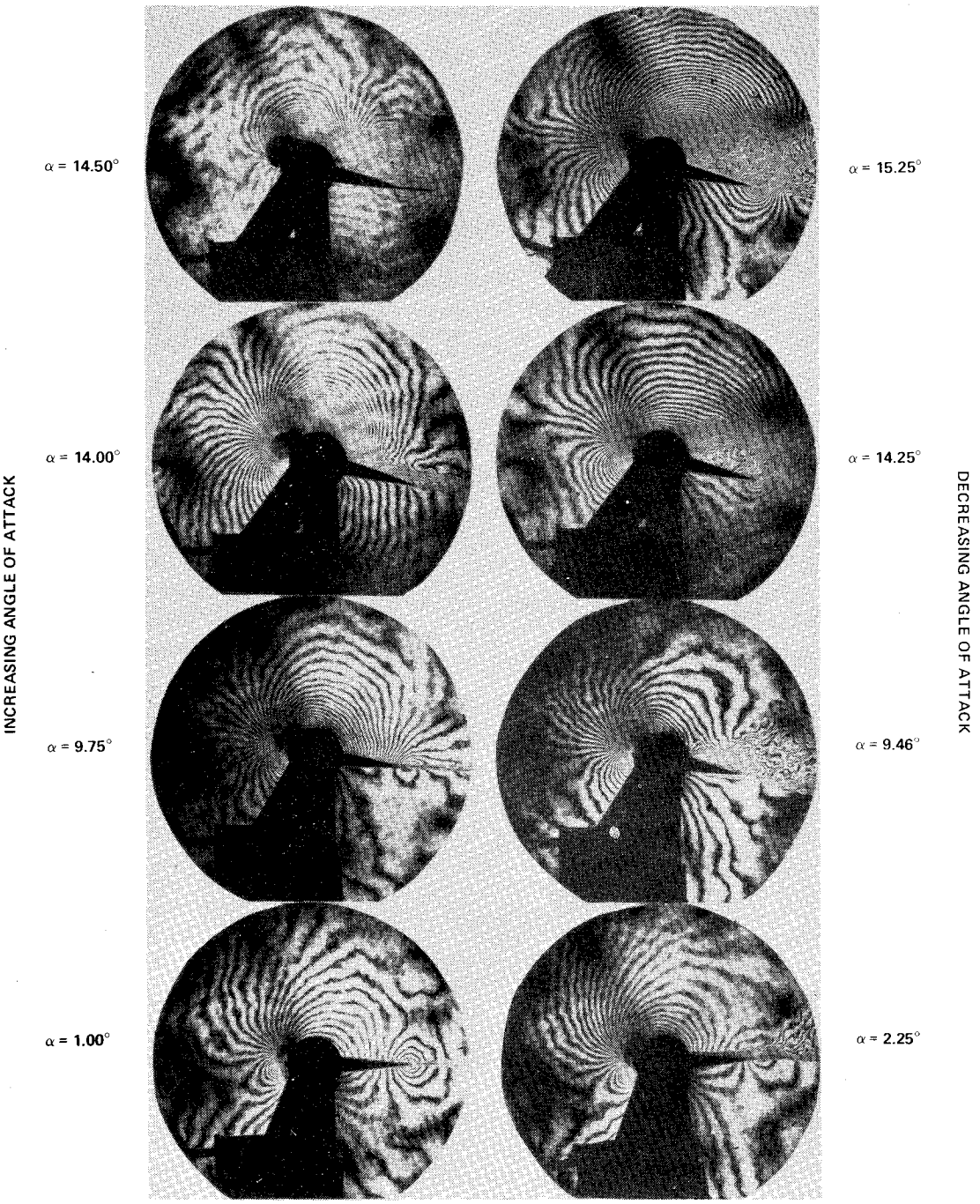

Fig. 4 Sequence of interferograms showing the airfoil going through dynamic stall.

The equation for the fringe shift is

$$\Delta\Phi(x,y) = \int_0^L [n(x,y) - n_0]\,dz = N\lambda \tag{1a}$$

and for two-dimensional flows, the change in index of refraction is

$$n(x,y) = n_0 + N\lambda/L \tag{1b}$$

The assumption of two-dimensional flow in this high height-to-chord ratio wind tunnel is valid for attached flows. This has been determined both experimentally and theoretically. For highly separated flows, the sidewall boundary layer can be separated and thus cause three-dimensional flows that would invalidate Eq. (1b). Using the Gladstone-Dale equation[5] that relates the refractive index of air to the density, the density can be shown to be

$$\rho(x,y) = N\lambda/kL + \rho_0 \tag{1c}$$

Once a particular fringe and its corresponding reference density are identified, the entire flowfield is determined.

The laser holographic interferometer at the 2- by 2-Foot Transonic Wind Tunnel at Ames Research Center has been described by Craig.[6] It is an off-axis system that incorporates a modern, 10 pps Nd:YAG pulsed laser; the laser provides reliable operation and is easy to align. A sketch of the interferometer with photographs of the laser, the transmitting and receiving optics, and the holographic plate is shown in Fig. 2. For the dynamic stall experiment or any unsteady flow

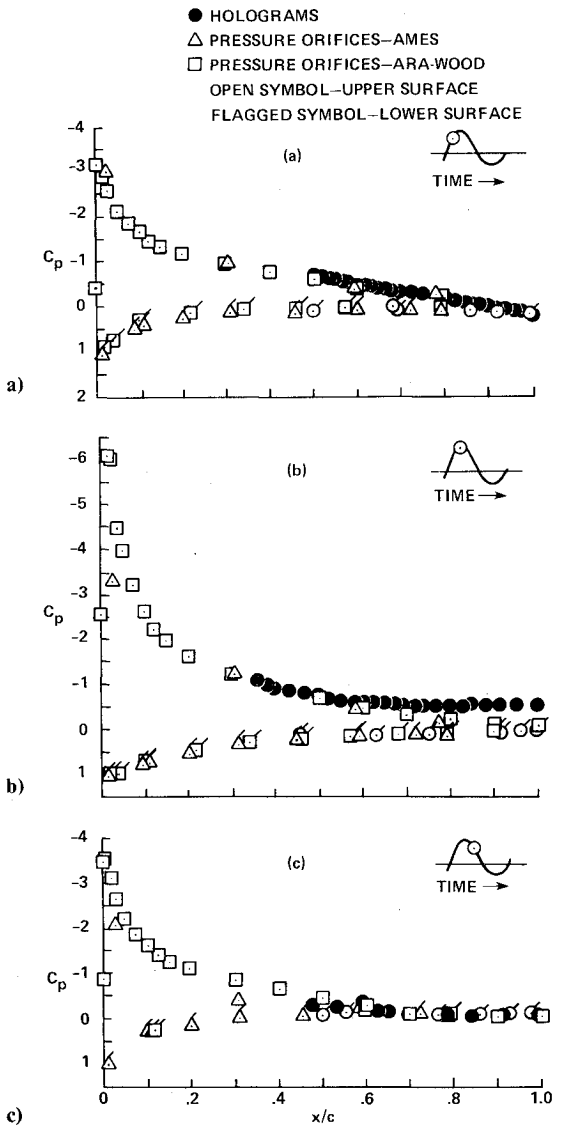

Fig. 5 Comparison of surface pressures from interferograms and orifices ($M=0.4$, $Re=2\times10^6$, $k=0.1$): a) attached flow, $\alpha=9.13$ deg; b) separated flow, $\alpha=14.39$ deg; c) reattaching flow, $\alpha=9.46$ deg.

applications, it is necessary to synchronize the laser pulse to an external event. The internal oscillator of the laser was replaced by an external one. If the external oscillator frequency is not within the 8-12 Hz range required for thermal equilibrium in the Nd:YAG rod, the source frequency must be multiplied or divided in a synchronous manner by integer amounts to achieve the proper frequency range. In this experiment, the airfoil was driven in pitching oscillation at frequencies of 10-40 Hz. For the airfoil images to coincide in the infinite fringe interferograms, both reference and object hologram must be recorded at the same airfoil position. The laser triggering was synchronized to an encoder signal from the airfoil pitch drive motor. Using an adjustable time delay, flow-on and flow-off holograms were recorded at repeatable airfoil positions throughout the oscillation cycle for the range of frequencies considered.

Reconstruction of Dual-Plate Interferograms

A typical reconstruction sequence of dual-plate interferograms to the final desired infinite fringe mode is shown in Fig. 3. This is for a symmetric NACA 0012 airfoil at $\alpha=1$ deg. At the first stage of reconstruction (Fig. 3a), the object and reference plates are placed in the dual-plate holder and

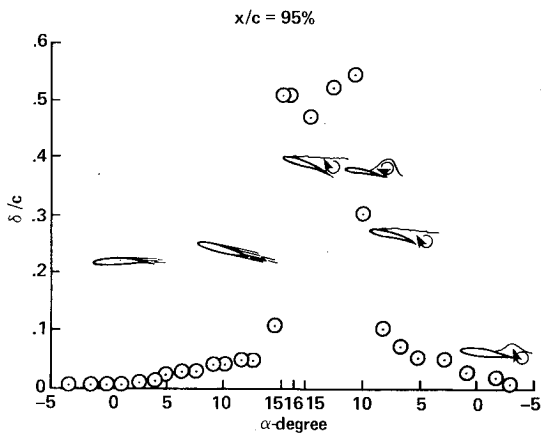

Fig. 6 Boundary-layer thickness and shear-layer thickness as airfoil goes through dynamic stall ($M=0.4$, $Re=2\times10^6$, $k=0.1$, $x/c=95\%$).

the airfoil and oscillating mechanism, that is, the dark shapes, are superimposed. The large number of fringes is typical of finite fringe interferograms. The second stage involves small movements of one plate with respect to the other, both to minimize the number of fringes and to achieve a fringe pattern based on a general knowledge of the aerodynamics. In this case, the symmetric airfoil at $\alpha=1$ deg should give a fringe pattern that is nearly symmetric to the horizontal plane of symmetry of the airfoil. The second-stage interferogram (Fig. 3b) shows fair symmetry except for the one fringe that crosses the airfoil at about 75% chord. It is further noticed that there are a number of vertical fringes behind the airfoil; these fringes indicate a change in density that should not occur. The final stage consists of minor adjustments to get rid of these vertical fringes and to minimize the number of fringes in the outer regions surrounding the airfoil, since these regions should have the smallest density gradients. Figure 3c shows the final infinite fringe interferogram used for data analysis.

This method of alignment requires the model to be sufficiently small so that the flow approaches the freestream density at some point near the edge of the interferogram. By definition, the fringe spacing becomes infinite when the density is at the freestream value. However, there is some subjectivity in this procedure for subsonic speeds since the density is never quite freestream and the noise of the system introduces two- or three-board fringes. For the experiment, the size of the model was determined from previous experiments and based on the agreement of the interferometric data with pressure orifice data.

Results

A typical sequence of infinite fringe interferograms of the airfoil going through one cycle of oscillation is shown in Fig. 4. Surface pressures, boundary layer, and wake profiles were measured from interferograms at a Mach number of 0.4, Reynolds number of 2×10^6, and reduced frequency of 0.1. The dynamic stall process, with the formation of the vortex, its shedding, and reattachment of the flow, can also be determined.

Figure 5 shows the comparison of surface pressures as measured from the interferograms and pressure orifices at three points of the cycle: an attached flow, a separated flow, and a reattaching flow. The digitizing of the fringes was done using an electronic digitizer connected to a minicomputer. This made the tedious digitizing task easier—a pressure distribution plot could be obtained in 15 min or less. Since

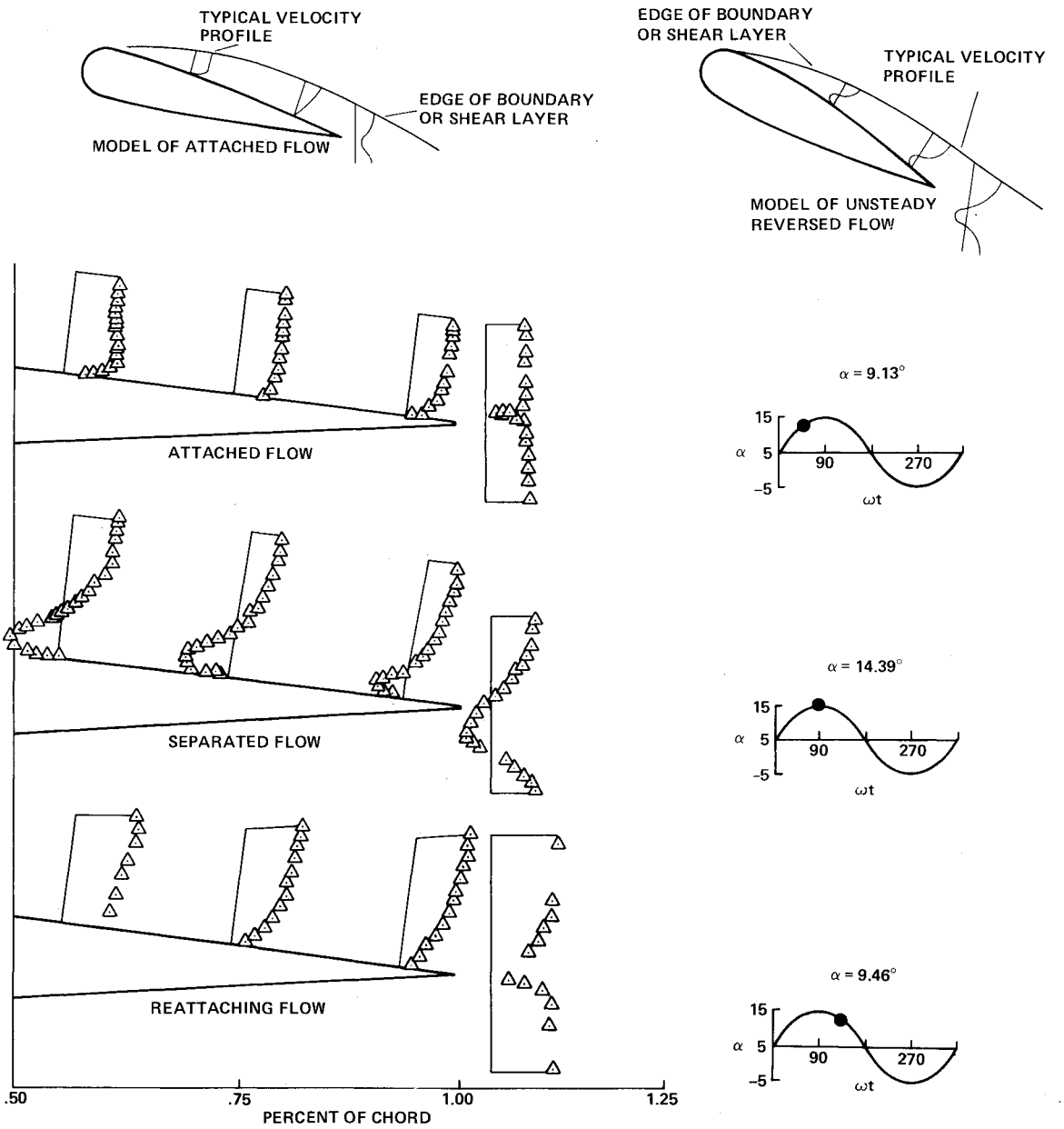

Fig. 7 Interferometric velocity profiles ($M = 0.4$, $Re = 2 \times 10^6$, $k = 0.1$).

interferometric data were available for the rear half of the airfoil, the pressure distributions of Wood[7] were added for qualitative comparison since Wood's data were obtained at slightly different test conditions. The agreement of the interferometric and orifice data is about 1% for the attached flow and reattaching flow cases. For the separated flow cases, the agreement is poor, and the interferometric technique for measuring surface pressures apparently does not work. The reason for the poor agreement is due to normal pressure gradients in the separated flow region. Examination of the interferograms reveals that large vortices are being shed in the separated flow region and that such vortices will produce normal pressure gradients. This invalidates the interferometric technique used to obtain the pressure along the inviscid boundary by fringe counting [see Eq. (1c)] and by assuming a constant normal pressure gradient. This assumption is the equivalent to saying that the separated flow behaves like a boundary layer. In this case, the assumption was a poor one. This result is different from previous results[8] on separated flow. Obviously, a method that can account for the effects of the vortex must be developed before the pressures can be obtained by interferometry.

Boundary-layer and separated flow thickness were measured over the rear half of the airfoil. The leading edge of the airfoil can be seen (Fig. 4), but most of the front half of the airfoil is obscured by the oscillating apparatus. The boundary layer and its edge can be easily defined. For example, as seen in Fig. 4, the fringes within the boundary layer are quite thin and closely spaced because of the large density gradients within the boundary layer. Another factor that helps in defining the boundary layer is that the density gradients in the outer inviscid region are approximately normal to the density gradients in the boundary. Using the above criteria, the boundary-layer thickness and the thickness of the separated flow region were determined. The thickness of the separated flow region was not as well defined and could be off several fringes in the dual-plate interferograms. Therefore, the double-pulse interferograms, which gave better definition of the edge of the separated flow, were used for separated flows.

A plot of the boundary-layer and separated flow thickness at the 95% chord station for one complete cycle of oscillation from -5 to $+15$ deg is presented in Fig. 6. At the start of the cycle, the boundary-layer thickness is about 0.7% of the

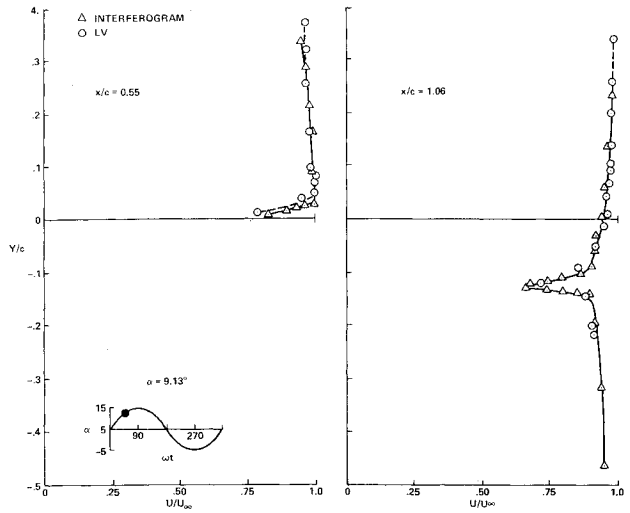

a) Attached flow.

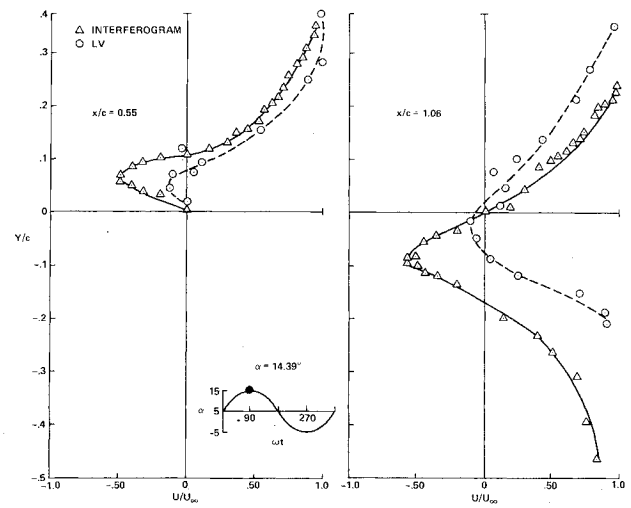

b) Separated flow.

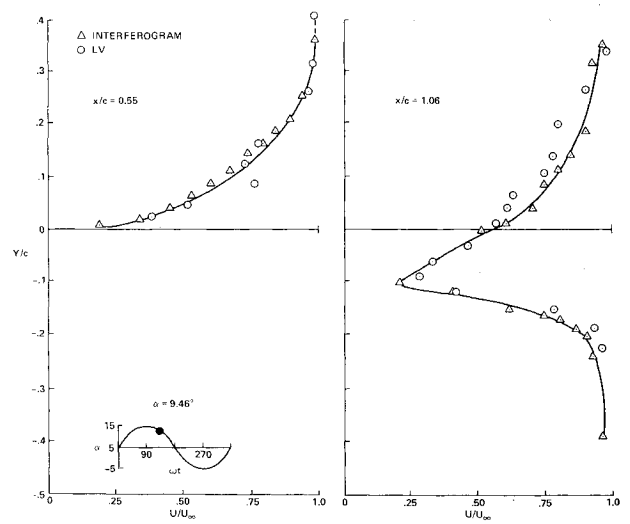

c) Reattaching flow.

Fig. 8 Comparison of velocity profiles with laser velocimetry data ($M=0.4$, $Re=2\times10^6$, $k=0.1$).

Fig. 9 Double-pulse interferogram ($M=0.6$, $Re=4\times10^6$, $\alpha=15.1$ deg, $k=0.05$).

chord, and it grows with increasing angle of attack to nearly 5% of chord at the onset of stall at about 14.0 deg. Up to this angle, the boundary-layer velocity profiles do not show any separated flows. At 14 deg, the layer grows to 11% of the chord and there is a small vortex near the midchord of the airfoil (see Fig. 4, $\alpha=14.0$ deg). At angles slightly above 14 deg, stall occurs, the flow separates, and a large vortex sweeps over the top of the airfoil. This seems to indicate a trailing-edge type of stall. This result is based on the observation of many interferograms. After stall, the flow thickness is nearly 60% of the chord. At this point in the cycle and with decreasing angles, the separated flow region decreases until complete reattachment occurs at an angle of attack of about -1 deg. Examination of the interferograms indicates that the large dynamic stall vortex has been replaced by several smaller ones. These vortices are continually swept downstream and disappear when reattachment occurs.

Velocity profiles at three chordwise stations and slightly into the wake were measured for the attached flow, separated flow, and reattaching flow cases. Velocity profiles were derived from the density, using the Crocco equation,[9]

$$\frac{T}{T_e}=1+r\frac{\gamma-1}{2}M_e^2\left[1-\left(\frac{u}{u_e}\right)^2\right]+\frac{T_w-T_{ad}}{T_e}\left(1-\frac{u}{u_e}\right) \quad (2)$$

and the perfect gas law. With the assumption that the wall temperature is adiabatic, Eq. (2) becomes

$$\frac{u}{u_e}=\left\{1-\frac{2[(T/T_e)-1]}{r(\gamma-1)M_e^2}\right\}^{1/2} \quad (3)$$

Constant pressure in the boundary layer was also assumed in the Crocco derivation. Figure 7 shows the velocity profiles data from the interferograms and Carr's flow model for attached and separated flows. The models from Carr et al. were based on experimental measurements such as smoke data. Overall, the interferometric profiles are similar to those of the model. (It is assumed that the reattaching flow is an attached flow case.) A closer examination of the interferometric data from the midchord to about 85% chord for attached and reattaching cases identifies two problems: 1) the velocity does not go to zero at the surface, as expected; and 2) the large velocity gradient at the surface that is typical of turbulent boundary layers is not seen. The cause of both problems is the bending of the airfoil caused by aerodynamic forces—the bending blocks the fringes near the surface. For a turbulent profile, there should be a large number of fringes near the surface because of the large density gradients. This

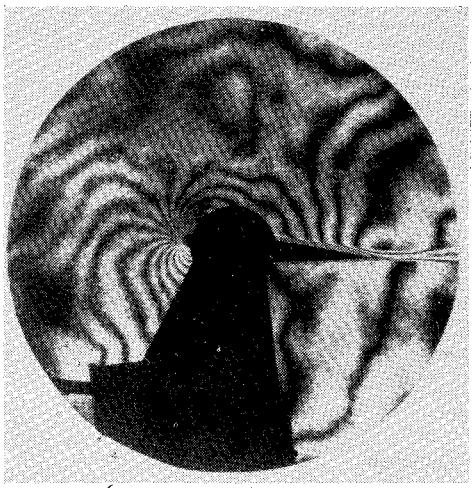

a) $Re = 1 \times 10^6$, $M = 0.4$, α (ascending) = 10 deg, $k = 0.1$.

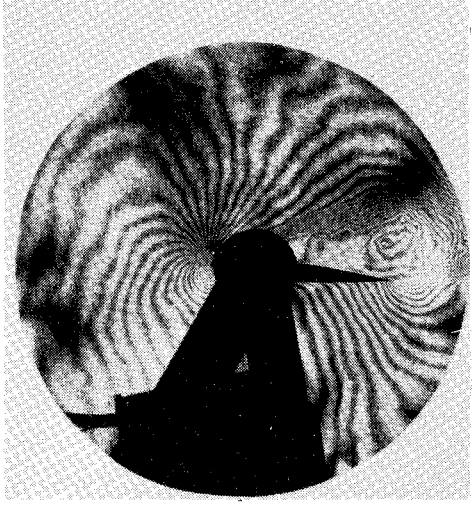

b) $Re = 1.5 \times 10^6$, $M = 0.6$, α (ascending) = 15 deg, $k = 0.05$.

Fig. 10 Interferograms at lower Reynolds number.

problem disappears in the wake and is not as crucial near the trailing edge, because the gradients there are mild and only one or two fringes are lost because of model bending.

Velocity profiles at the midchord and the near-wake determined with laser velocimetry (LV) by Owen[10] and with interferometry agreed very well for the attached and reattaching flows (see Figs. 8a and 8c). Note that the interferometric technique measures the speed by integrating along a path across the test section. On the other hand, the velocimeter measures a time-averaged, two-component velocity at a point. For steady two-dimensional flow, these two measurements should agree. For unsteady two-dimensional flows with velocity fluctuations or rms values as high as 35% of the freestream velocity, one would expect the mean velocity from a temporal and spatial technique to agree only if a sufficient amount of data was taken. For the LV data, about a thousand particle events were used in the averaging. No number could be given for interferometry, but is assumed that it is large over a 2 ft beam path. The closest distance to the airfoil surface that could be measured by the velocimeter was about 0.06 in. For the separated flows (Fig. 8b), the agreement between the two methods is poor. Again, as in the caculation of surface pressures, the basic assumption of zero pressure gradients in the normal direction, used in deriving the Crocco equation, was violated. Another basic assumption, that of constant total enthalpy, was also violated as a result of the unsteady flow.

A typical double-pulse interferogram is presented in Fig. 9. The separated flow region and the wake exhibit large numbers of fringes because of the density fluctuations occurring within the time of the laser pulses—about 0.1 ms. Outside the separated region and the wake, the density remains essentially constant during this time; therefore, there are very few fringes in these regions. As a result, the boundaries of the wake and separated regions are much better defined in the double-pulse interferograms. Note that double-pulse data are qualitative in nature.

Interferograms were also taken at a lower Reynolds number (1×10^6). As expected, the number of fringes is reduced. According to Eq. (1c), the reduction in fringes is directly proportional to the magnitude of the density. As seen in Fig. 10, the boundary layer, separated flow region, and wake structure are well defined. The lack of fringes would affect the accuracy, the velocity profiles, and further reductions in densities could affect the usefulness of the interferometric technique.

Summary

Laser holographic interferometry was tried as a nonintrusive diagnostic tool for studying unsteady two-dimensional flows. A NACA 0012 airfoil was tested, while undergoing dynamic stall, over a range of Mach numbers of 0.3-0.6, Reynolds number os $0.5\text{-}2 \times 10^6$, and reduced frequencies of 0.015-0.15. It was found that both quantitative and qualitative data could be obtained by the technique. Surface pressures on the airfoil can be measured to within 1% of those measured with orifices and pressure transducers when the flow is attached. Velocity profiles were measured near the wake region, and they compared very well with laser velocimeter data for attached flows. For separated flows with large-scale vortices, densitities can be measured, but pressures and velocities cannot be deduced with the assumption of constant-pressure gradient in the normal direction. The sensitivity of the interferograms was good at a Mach number of 0.4 and a Reynolds number of 4×10^6/ft; the sensitivity worsened at smaller Mach numbers and Reynolds numbers, and improved at larger ones.

References

[1] Carr, L. W., McAlister, K. W., and McCroskey, W. J., "Analysis of the Development of Dynamic Stall Based on Oscillating Airfoil Experiments," NASA TN D-8382, 1977.

[2] Werle, H., "Hydrodynamics Flow Visualization," *Annual Review of Fluid Mechanics*, VS, edited by M. VanDyke and W. G. Vincenti, Annual Review Inc., Palo Alto, Calif., 1973, pp. 361-380.

[3] Werle, H., "Flow Visualization Techniques for the Study of High Incidence Aerodynamics," AGARD, Von Kármán Institute Lecture Series 121, March 1981,

[4] McAlister, K. W. and Carr, L. W., "Water Tunnel Visualization of Dynamic Stall," *Transactions of the American Society of Mechanical Engineers*, Vol. 101, 1979, pp. 376-380.

[5] Vest, C. M., *Holographic Interferometry*, John Wiley & Sons, New York, 1979, pp. 254-284.

[6] Craig, J. E., "Operating Manual Holographic Interferometry System for 2- by 2-Foot Transonic Wind Tunnel," NASA CR-166344, 1981.

[7] Wood, M. E., "Results of Oscillatory Pitch and Ramp Tests on the NACA 0012 Blade Section," Aircraft Research Association Ltd., Bedford, England, Memo 220, 1979.

[8] Johnson, D. A. and Bachalo, W. D., "Transonic Flow about a Two-Dimensional Airfoil—Inviscid and Turbulent Flow Properties," AIAA Paper 78-1117, 1978.

[9] Schlicting, H., *Boundary Layer Theory*, McGraw-Hill Book Co., New York, 1960, p. 346.

[10] Owens, F. K., private communication, Complere Inc., 1982.